Tectonophysics 666 (2016) 23–32

Contents lists available at ScienceDirect

Tectonophysics

journal homepage: www.elsevier.com/locate/tecto

Stress adjustment revealed by seismicity and earthquake focal mechanisms in northeast China before and after the 2011 Tohoku-Oki earthquake

Hongyu Yu [a,b,*], Li Zhao [c], Yajing Liu [b], Jieyuan Ning [a], Qi-Fu Chen [d], Jian Lin [e]

[a] School of Earth and Space Sciences, Peking University, Beijing 100871, China
[b] Department of Earth and Planetary Sciences, McGill University, Montreal, QC H3A 0E8, Canada
[c] Institute of Earth Sciences, Academia Sinica, Taipei 115, Taiwan
[d] Key Laboratory of Earth and Planetary Physics, Institute of Geology and Geophysics, Chinese Academy of Sciences, Beijing 100029, China
[e] Department of Geology and Geophysics, Woods Hole Oceanographic Institution, Woods Hole, MA 02543, USA

ARTICLE INFO

Article history:
Received 13 March 2015
Received in revised form 25 September 2015
Accepted 7 October 2015
Available online 23 October 2015

Keywords:
Seismicity
Focal mechanism solutions
Regional stress field
Coulomb stress change
Tohoku-Oki earthquake
Northeast China

ABSTRACT

In order to understand the influence of the March 11, 2011, M_W 9.0 Tohoku-Oki earthquake on regional-scale seismicity, we study the seismicity rate and focal mechanism solutions (FMSs) of earthquakes in northeast China (NEC) before and after the megathrust event. Broadband seismic waveforms from 270 permanent and temporary stations are used to invert for the moment tensors of 69 earthquakes between 2009 and 2013 in the NEC. Our results show that there are distinct changes in seismicity rate on major NEC faults before and after the 2011 Tohoku-Oki event although the seismic moment rate of the whole region remains roughly constant. In comparison to a wide distribution of earthquakes before the Tohoku-Oki event, FMSs of crustal earthquakes in the NEC after the megathrust event can be categorized into two groups: strike–slip events with E–W compression and normal-faulting events with N–S extension. Stress field inversions before and after the Tohoku-Oki event suggest that the variations in seismicity and FMSs are due to a minor adjustment of regional stress state imposed by the megathrust event, which is further confirmed by static Coulomb stress change calculations. Mantle-depth seismicity is also influenced by the megathrust event, possibly via a down-dip transfer of compressional stress along the subducting plate, as manifested by the absence of moderate-sized mantle-depth earthquakes (~M_W 4–5) between May 2011 and April 2013 and the occurrence of deep-focus events with P axes along the dip direction of the subducting Pacific Plate in E–W vertical cross-sectional view and in WNW–ESE direction in map view.

1. Introduction

The March 11, 2011, Tohoku-Oki earthquake (M_W 9.0) ruptured an area of approximately 500 × 200 km^2 along the northeastern Japan megathrust (Ammon et al., 2011; Fujii et al., 2011; Hayes, 2011). Coseismic slip reached to more than 50 m near the trench (Yue and Lay, 2011; Simons et al., 2011; Shao et al., 2011; Ito et al., 2011), and was detectable in GPS measurements in a large area of East Asia (Shestakov et al., 2012; Hwang et al., 2012; Wang et al., 2011). Near-field static Coulomb stress change calculations have shown that some aftershocks were triggered by the coseismic stress perturbation (Toda et al., 2011a,b), and can be used to assist in the estimation of earthquake occurrence probabilities in Japan (Hiratsuka and Sato, 2011). However, it is not clear whether seismicity and stress in eastern China could be obviously influenced by the Tohoku-Oki event.

The Northeast China (NEC) region (Fig. 1a) has a prevailing low-level E–W compression (Ning and Zang, 1987; Xu, 2001), and is characterized by two conjugate fault systems (Fig. 1b): a NNE–SSW-trending right-lateral system, mainly containing the Nenjiang–Laohahe Fault (NLF), Central Songliao Basin Fault (CSBF), Yilan–Yitong Fault (YYF), Hunhe Fault (HF), and Dunhua–Mishan Fault (DMF); and a NW–SE-trending left-lateral system involving mainly the Chenshu–Boli Fault (CBF, Xu and Deng, 1996). The locations of these faults approximately control the spatial pattern of seismicity in the NEC (Fig. 2a).

Located more than 1200 km away from the Japan Trench (Fig. 1a), the NEC is a suitable area for studying the possible influence of a megathrust event on regional seismicity and stress field. In particular, this is the only region in China where deep-focus earthquakes (>350 km) are recorded as a result of the subduction of the Pacific Plate under the Eurasian Plate extending northwestward beneath NEC (Huang and Zhao, 2006). These deep-focus events allow us to simultaneously examine if and

* Corresponding author: School of Earth and Space Sciences, Peking University, Beijing 100871, China, and Department of Earth and Planetary Sciences, McGill University, Montreal, QC H3A 0E8, Canada.
E-mail addresses: 1101110441@pku.edu.cn, hongyu.yu@mail.mcgill.ca (H. Yu).

http://dx.doi.org/10.1016/j.tecto.2015.10.009
0040-1951/

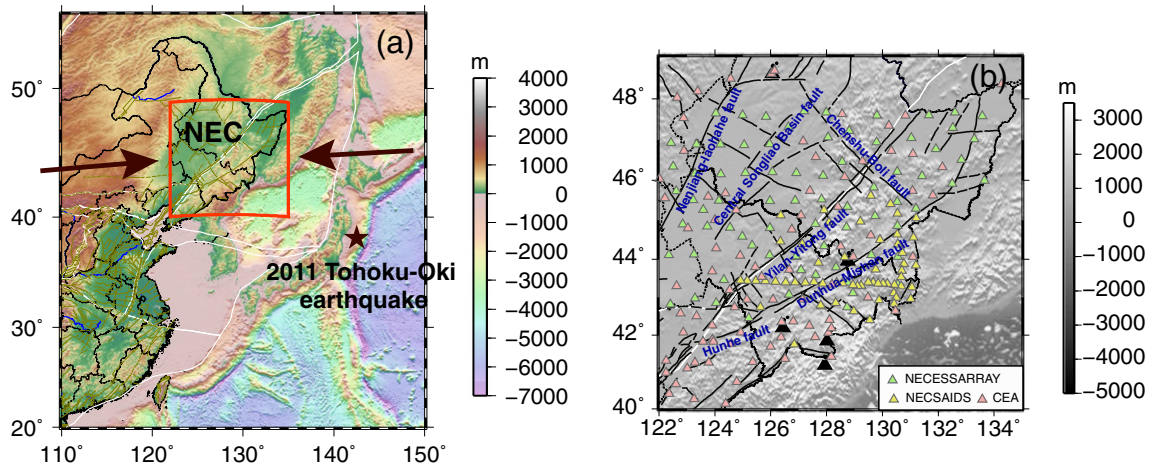

Fig. 1. (a) Topography of East Asia. Our study area, Northeast China, is indicated by the red box. The star marks the hypocenter of the 2011 Tohoku-Oki earthquake. Arrows indicate the direction of maximum compressional stress in the region, modified from Xu (2001). (b) Seismic station distribution in Northeast China. We used waveform records from stations of the NECESSARRAY (green) and NECSAIDS (yellow) temporary networks and the CEA (China Earthquake Administration) permanent stations (pink). Major faults are depicted by black lines (Deng et al., 2007), and locations of volcanoes are marked by black triangles.

how the megathrust event might influence the stress state at mantle-depth, as their epicentral distances to the Japan Trench are similar to those of the shallow events above them.

Previous statistics studies suggest that seismicity in the NEC has some relation with the activities in the Japan Trench, manifested by delayed seismic activities following large earthquakes in the Japan Trench area (Wu et al., 1979; Li and Wang, 1996; Gao, 2011), although clear descriptions and explanations are still lacking. However, recent Coulomb Failure Stress change (△CFS) computations show that the Tohoku-Oki earthquake is unlikely to significantly alter the stress field in the NEC (Cheng et al., 2014). Therefore, it is important to quantitatively analyze if a small △CFS (<0.01 MPa) might still have influence on the seismicity and the focal mechanism solutions (FMSs), in particular given the newly acquired high-quality data. Earthquake detectability in the NEC has improved tremendously during the last decade. As shown in Fig. 2(b), the number of detected events grows significantly, providing a more complete dataset for studying the regional response to a remote event in seismicity and the FMSs (Zheng et al., 2010). Moreover, temporary deployments of 129 stations of the NorthEast China Extended SeiSmic Array (NECESSArray, 2009–2011) and 60 stations of the NorthEast China Seismic Array to Investigate Deep Subduction (NECSAIDS, 2010–2013) provide additional data and greatly enhance our ability to study the seismicity and stress field in this region (Fig. 1b).

In this paper, we first report variations of seismicity around different geological units (major faults) in our study region before and after the Tohoku-Oki earthquake. Then we determine FMSs of moderate events by the generalized Cut and Paste (gCAP) method (Zhu and Ben-Zion, 2013) and use them to invert for the spatial and temporal variations

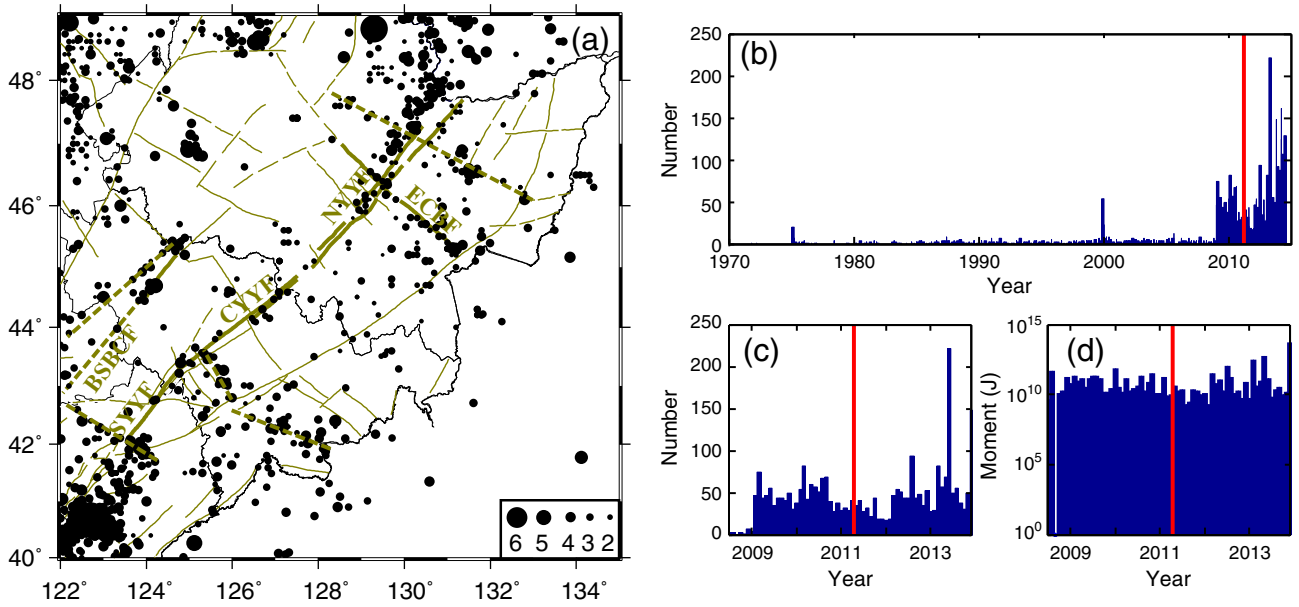

Fig. 2. Seismicity in northeast China. (a) Epicenters of 2024 earthquakes occurred before the Tohoku-Oki earthquake (1970–2011, $M_L \geq 1.0$) in our study area from the China Earthquake Network Center (CENC) catalog. The sizes of circles are proportional to event magnitudes. Green solid lines mark the faults in the NEC. In between, thick green solid lines show faults introduced in the text. Thick green dashed lines indicate the buried faults inferred from lineations in seismicity. (b) Monthly seismicity rate from the CENC catalog between 1970 and 2014. The red line marks the time of the 2011 Tohoku-Oki earthquake. (c) and (d) show the monthly seismicity rate and moment, respectively, between July 2008 and November 2013.

of regional stress field by applying the damped regional-scale stress inversion method (DRSSI; Hardebeck and Michael, 2006). Furthermore, we will calculate the static △CFS in the NEC due to the coseismic slip of the 2011 Tohoku-Oki earthquake (Toda et al., 2011a, 2011b, 2011c). Finally, these quantitative results will be used to analyze the influence of the megathrust earthquake on the seismicity and FMSs in the NEC.

2. Data and method

2.1. Earthquake catalog and waveform records in the NEC

For catalog analysis, we collect 3606 crustal-depth events (<35 km, $M_L \geq 1.0$) reported by the China Earthquake Network Center (CENC) between 1970 and 2014, and 644 mantle-depth events (>350 km, $M_b \geq 2.2$) reported by the International Seismological Centre (ISC) in the same period. For crustal-depth events, we use the CENC catalog rather than the ISC catalog, because ISC employs the global seismic networks with coverage that is not as dense as CENC for recording small shallow earthquakes ($M_L < 3$) at a high level of completeness in our study area.

For waveform analysis, we use broadband seismic records from three regional networks to determine the focal mechanism solutions. These include 116 permanent stations of the China Earthquake Administration (CEA, 2009–2013, Zheng et al., 2010), 129 temporary stations of the NorthEast China Extended SeiSmic Array (NECESSArray, 2009–2011) and 60 stations of the NorthEast China Seismic Array to Investigate Deep Subduction (NECSAIDS, 2010–2013), as shown in Fig. 1(b). We collected waveforms of earthquakes with magnitude $M_L \geq 2.9$ in the NEC region reported by CENC from December 2009 to May 2013. During this period, 119 earthquakes in total are selected for focal mechanism analysis.

2.2. Earthquake focal mechanism calculation

The focal mechanisms of moderate and large earthquakes ($M_W > 5$) are now routinely determined by waveform inversion in the global CMT catalog (Ekstrom et al., 2012). Waveform inversion relies on accurate earthquake locations and velocity models in order to calculate Green's functions to obtain reliable moment tensor solutions (e.g., Patton and Zandt, 1991; Dreger and Helmberger, 1993; Romanowicz et al., 1993; Zhao and Helmberger, 1994; Zhu and Helmberger, 1996; Herrmann et al., 2011; Zhu and Ben-Zion, 2013). However, the crustal velocity structure of the NEC region has not been extensively studied, and the majority of the NEC earthquakes are of small to moderate sizes (i.e., magnitude 3–5), with source locations that are not well constrained. Therefore, we choose the generalized Cut and Paste method (gCAP) of Zhu and Ben-Zion (2013) to determine the FMSs.

The gCAP method, first developed by Zhao and Helmberger (1994) and Zhu and Helmberger (1996), has the advantage of fitting P and S waveforms simultaneously during inversion, thus relying much less on the accuracy of earthquake locations and velocity structures. Zhu and Ben-Zion (2013) further generalized the method to include the non-double-couple source components. The moment tensor can thus be decomposed into three source terms: isotropic (ISO), double-couple (DC) and compensated linear vector dipole (CLVD). Two dimensionless parameters ζ_m and χ are introduced to quantify the weights of the ISO and CLVD components, respectively. The seismic moment tensor M_{ij} of an earthquake point source is expressed as (Zhu and Ben-Zion, 2013)

$$M_{ij} = \sqrt{2} M_0 \left(\zeta_m I_{ij} + \sqrt{1-\zeta_m^2} \left(\sqrt{1-\chi^2} D_{ij}^{DC} + \chi D_{ij}^{CLVD} \right) \right), \quad (1)$$

where I_{ij} is the 2nd-order identity tensor, D_{ij}^{DC} and D_{ij}^{CLVD} are normalized DC and CLVD moment tensors, respectively, and M_0 is the seismic moment. Thus, a complete description of the moment tensor is given by six independent parameters: three scaling factors, M_0, ζ_m and χ, and the three angles, strike ϕ, dip δ and rake λ, for the orientations of the fault plane and coseismic motion, which determine the deviatoric components D_{ij}^{DC} and D_{ij}^{CLVD}.

In order to obtain synthetic waveforms efficiently, gCAP adopts the frequency-wavenumber integration approach (Aki and Richards, 2002; Zhu and Rivera, 2002) to compute the Green's functions in a one-dimensional (1D) layered velocity model. We adopt a layered velocity model (see Fig. 3) that combines velocity structures for the upper 35 km from a regional tomography study (Sun, 2005) and from the global AK135 model (Kennett et al., 1995) for depths below 35 km. During the inversion, three-component waveform records are cut into five phase windows, including vertical and radial components of P wave and all three components of S wave windows.

We then use the gCAP method to fit the recorded and synthetic waveforms in all phase windows simultaneously by grid search. This approach enhances the weight of P waveforms, as compared to the whole-waveform inversion in which S waveforms are the dominant features to fit due to their much larger amplitudes. Time-shifts between the synthetics and records of different phases can be used to adjust for the deviations of travel times and earthquake location from their true values. Window lengths for P and S waves are chosen as 35 s and 70 s, respectively, while the frequency bands are 0.05–0.3 Hz and 0.02–0.1 Hz (Zhao and Helmberger, 1994). Moreover, we use a factor of 2 for the weight of P wave relative to S wave for distance scaling, and adopt grid spacing values of 2 km in depth, 6° in strike, dip and rake angles, and 0.02 for both the scaling parameters of the ISO and CLVD components.

Thresholds of correlation coefficients between the recorded and synthetic seismograms are set as 65% for P wave and 70% for S wave. Moreover, the focal mechanisms are determined with at least 15 waveform windows. After applying the above criteria, we obtain the FMSs of 69 earthquakes out of the 119 $M_L \geq 2.9$ events.

2.3. Stress orientation inversion

Earthquake focal mechanisms provide seismological constraints on the stress orientations in the hypocentral region. Assuming that the slip vector is parallel to the shear traction on the fault plane and the magnitude of the shear traction on each plane that ruptures is similar, the components of the unit slip vector and those of the stress tensor have a linear relationship (Michael, 1984). To quantitatively examine the stress change due to the 2011 Tohoku-Oki earthquake, we also

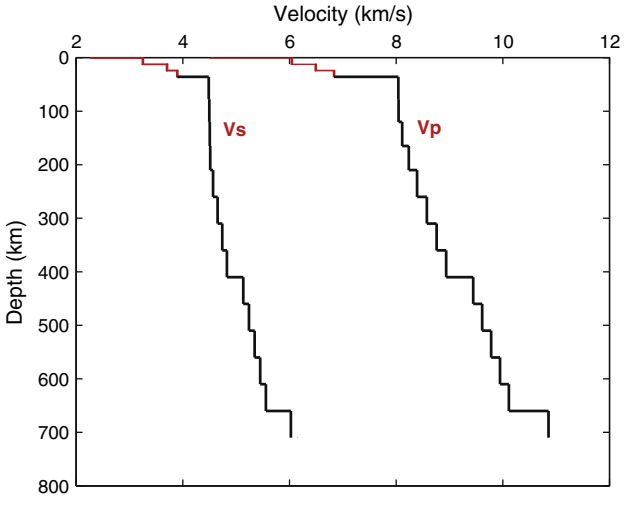

Fig. 3. 1D layered velocity model for Green's function calculation. The model contains the structures of Sun (2005) for the upper 35 km (red) and the AK135 model (converted to uniform layered structure) at greater depths (black).

conduct a stress inversion based on the FMSs. We use the damped regional-scale stress inversion (DRSSI) method of Hardebeck and Michael (2006), which seeks a least-squares solution of the inverse problem,

$$\left(\mathbf{G}^{\mathrm{T}}\mathbf{G} + e^2\mathbf{D}^T\mathbf{D}\right)\mathbf{m} = \mathbf{G}^T\mathbf{d}, \quad (2)$$

where **m** is the model vector consisting of stress tensor components on all the grid points and **d** is the data vector involving the slip components of all the focal mechanisms. **G** is the data kernel matrix derived from the fault normal vector of all focal mechanisms. **D** is the damping matrix and e is the damping coefficient. The damping term suppresses the difference between the stress tensor elements at adjacent grid points, thus allowing for a regional inversion without the need for subjective division of earthquakes (Hardebeck and Michael, 2006).

The grid size used in stress tensor inversion depends on the spatial density of the available FMSs. In this study, we only have 36 events before and 33 after the megathrust event that can be used in the stress field inversion. After testing different grid sizes, we use the relatively stable and reliable grid size of 2.0° in longitude and 1.0° in latitude. We invert the stress orientations of crustal-depth and mantle-depth events separately, and give half weight to lower-quality FMSs. Although most of the grids relate less than five earthquakes (Table S2 in supplementary material shows the number of mechanisms applied per grid), the stress state in each grid is consistent with its neighboring grids, which means that they do not change abruptly across grid. Due to the large epicentral distance (1200 km), the inverted apparent stress field that we discuss in this paper is a manifestation of the stress adjustment on seismic faults in NEC due to the 2011 Tohoku-Oki earthquake. Thus, the inverted stress state is still resolvable although its implications need to be carefully treated.

The inverted result is also confirmed by our bootstrap test result. A bootstrap method in software MSATSI (Martínez-Garzón et al., 2014; Hardebeck and Michael, 2006; Lund and Townend, 2007) are applied here to estimate the uncertainty of our results. We randomly generate 200 resamplings of the original dataset for crustal- and mantle-depth earthquakes. The uncertainties are determined assuming 95% confidence intervals. The bootstrap test results show that the orientations of P-, N- and T-axes of stress inversion on each grid are concentrated respectively in stereonet view, suggesting that the results of stress state inversion is stable and resolvable. For more detailed descriptions about the procedure of inversion and corresponding bootstrap tests, please refer to Supplementary Material Fig. S1.

3. Results

3.1. Seismicity and focal mechanism solutions in the NEC

The seismicity in the NEC between July 2008 and November 2013 is shown in Fig. 4. We collected 2857 earthquakes of $M_L \geq 1.0$ from CENC, in which 1275 events occurred before the 2011 Tohoku-Oki earthquake. In general, the level of seismicity throughout NEC is relatively low compared to other seismically active zones, such as North China, and the largest shallow-focus earthquake within the spatial–temporal range of our study is M_L 4.2. As shown in Fig. 2(c) and (d), both the seismicity rate and total moment do not vary much before and after the 2011 Tohoku-Oki earthquake. Besides, the spikes in seismicity around 2013 and 2014 in Fig. 2(c) is probably due to the local earthquake on 22 April 2013 (M_L 5.3, 122.3°E, 42.9°N; see Fig. 4), resulting in a brief period (about two weeks) of seismicity increase within the surrounding area. The total moment (Fig. 2d) does show a normal fluctuation, rather than a sharp increase, around the same period.

However, in the vicinity of major faults marked by the green boxes in Fig. 4(a), there is a noticeable change in crustal seismicity rate. Taking

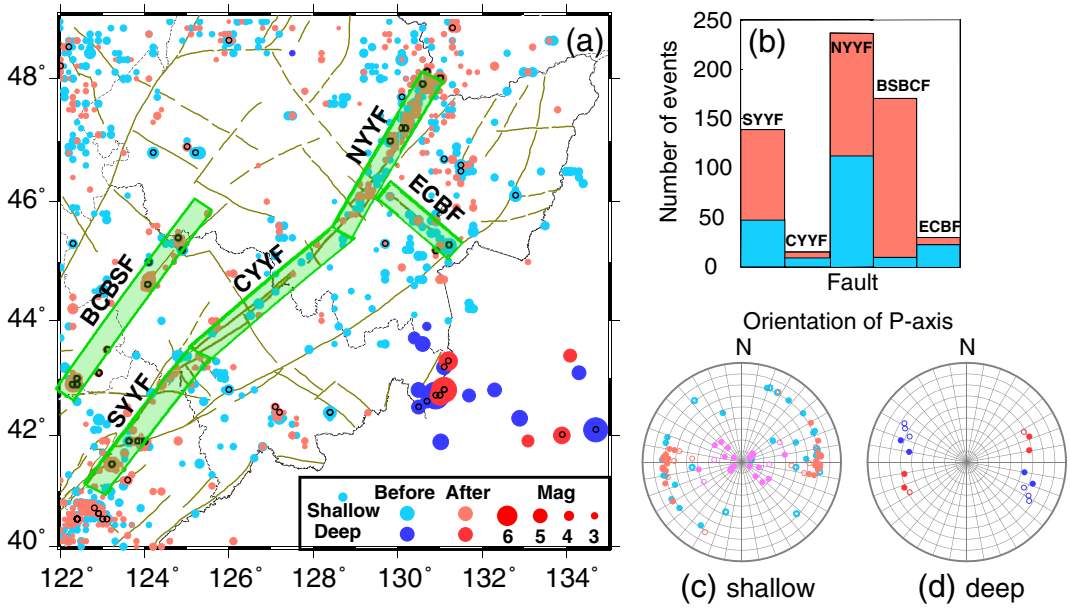

Fig. 4. Seismicity and earthquake P axes between 2008 and 2013 in Northeast China. (a) Distribution of 2857 earthquakes of $M_L \geq 1.0$ from July 2008 to November 2013. The epicenters are shown in circles with blue and pink colors for events occurred before (1275) and after (1582) the 2011 Tohoku-Oki earthquake, respectively, and lighter and darker colors for crustal- (<50 km) and mantle-depth (>350 km) earthquakes, respectively. The sizes of circles are proportional to event magnitudes. The earthquakes for which we calculated FMSs are indicated by the open black circles. Green belts mark the fault zones we focus on in this study. Taking the uncertainty of both earthquake locations and fault traces into consideration, we choose a width of 50 km for the fault zones here. (b) Histogram of seismicity in the fault zones in (a), plotted with the same color sch. as in (a). The number of earthquakes in fault zones SYYF, CYYF, NYYF, BSBCF, and ECBF before/after the 2011 Tohoku-Oki earthquake are 47/92, 9/6, 113/124, 10/161, 23/7, respectively. (c) Stereo map of P axes for shallow-focus events before and after the 2011 Tohoku-Oki earthquake, based on our result of gCAP focal mechanism solutions. Blue circles are for the P axes of earthquakes occurred before the 2011 Tohoku-Oki earthquake. Red and magenta circles are for E–W-striking and N–S-striking normal-fault earthquakes, respectively, after the megathrust earthquake. Solid and open circles are for P axes of higher- and lower-quality focal mechanisms, respectively. (d) P axes for deep-focus events. Blue and red circles are respectively for P axes of earthquakes occurred before and after the 2011 Tohoku-Oki earthquake. Open circles are for earthquakes of smaller magnitudes ($M_W < 5.5$).

the uncertainties in both earthquake locations and fault geometries into account, we conduct a statistical analysis using events in a 50-km wide zone along each fault as shown in Fig. 4(a). The result in Fig. 4(b) shows that the number of events clearly increases along southern YYF (SYYF), and buried CSBF (BCSBF), slightly increase along northern YYF (NYYF), while decreases along the central part of the YYF (CYYF), and the eastern part of the CBF (ECBF).

At the mantle depths, Fig. 5(a) shows the deep earthquakes in the NEC between 1970 and 2014, which indicates that the ISC catalog has a lower magnitude detection threshold than that of CENC, as it records many smaller deep-focus earthquakes around the level of magnitude 3. Furthermore, the number of reported events had a sharp increase in 1995 due to the improvement of monitoring ability. Thus, our discussion for deep-focus earthquakes will be based on the 1995–2014 ISC catalog, as shown in Fig. 5(b). There is an apparent lack of moderate earthquakes (magnitude 4–5) from May 2011 to April 2013, which might be due to the stress field adjustment related to the 2011 Tohoku-Oki earthquake since the gap began shortly after it. We will discuss its possible mechanism in the Discussion section.

We determined 69 FMSs ($2.9 \le M_W \le 6.8$) of events from December 2009 to May 2013 by the gCAP method, including 36 earthquakes before the 2011 Tohoku earthquake, and 33 after (see Fig. 6 and the supplemental material Table S1 for detailed information). The dense distribution of stations employed in this study helps constrain the moment tensor solutions down to magnitude 2.9. Two additional focal mechanism solutions reported in the GCMT catalog after May 2013 are also included in Fig. 6.

As Fig. 4(c) shows, before the 2011 Tohoku-Oki earthquake, the directions of the P axes in the crust are diverse, which strongly depend on the local stress state and are weakly controlled by the background low-level E–W compression. After the megathrust event, however, the P axes of the strike–slip events rotated to roughly E–W orientation. By comparison, the horizontal component of P axes of large deep-focus earthquakes rotated anticlockwise after the Tohoku-Oki event from WNW–ESE to WSW–ENE. We highlight in Fig. 4(d) the P axes of events of $M_W > 5.5$ with solid circles while smaller events with hollow circles, as the FMSs of the larger deep events are more precisely determined and more representative of the regional stress state.

3.2. Stress adjustment due to the 2011 Tohoku-Oki earthquake

The inversion results of the stress field before and after the 2011 Tohoku-Oki earthquake are shown in Fig. 7(a) and (b), respectively. Horizontal projections of the principle stress axes σ_1 (maximum compression) and σ_3 (minimum compression) are plotted at each resolvable grid point. The observable change in the stress orientation of stress field, although the changes might not be large, is consistent with the observation of seismicity rate. The epicentral distance of NEC area is more than 1200 km, resulting in small changes in stress amplitude (as shown by our Coulomb failure stress change result will shows in Section 3.3) but observable rotation of P axes (Fig. 4c and d). Moreover, the effect of the 2011 Tohoku-Oki earthquake on stress state of seismic faults in the NEC is roughly a horizontal E–W extension, paralleled to the orientation of P axes. Therefore, we focus on discussing the rotation of P axes orientation in this study.

We highlight four areas with various types of noticeable variations in Fig. 7. In the north of our study area (marked by gray ellipses), the direction of maximum compression rotated from roughly E–W to WNW–ESE, parallel to the P axis of the 2011 Tohoku-Oki megathrust event. In the area marked by purple ellipses, the level of background horizontal compression is relatively low before the 2011 Tohoku-Oki earthquake, while after the megathrust event, the direction of σ_1 became much more uniform, with a more-or-less horizontal and E–W orientation. In the southwest corner (marked by orange ellipses), on the other hand, the direction of σ_1 became almost vertical after the Tohoku-Oki event, which indicates a release of horizontal stress in that area. Chen et al. (2012) presented the coseismic GPS observations in the NEC induced by the 2011 Tohoku-Oki earthquake based on GPS observation. Their coseismic strain result also shows sub-horizontal E–W extension at crustal-depth, which agrees with our stress state inversion as shown in Fig. 7(b). Comparatively, the horizontal projections of σ_1 indicated by the mantle-depth earthquakes (marked by green circles) changed from WNW–ESE to WSW–ENE after the Tohoku-Oki earthquake.

3.3. Static Coulomb failure stress change

To quantify the effect of the 2011 Tohoku-Oki earthquake on the faults in the NEC, we also calculate the Coulomb Failure Stress change (△CFS) on the major faults there using Coulomb 3.3 (Toda et al., 2011a; Lin and Stein, 2004; Toda et al., 2005). △CFS in our study is defined as

$$\Delta CFS = \Delta\tau - \mu \cdot \Delta\sigma_n, \tag{3}$$

where $\Delta\tau$, $\Delta\sigma_n$ are the changes in shear and normal stresses respectively (positive for compression), and μ is Coulomb frictional coefficient (King et al., 1994). Due to the large epicentral distance, differences in the

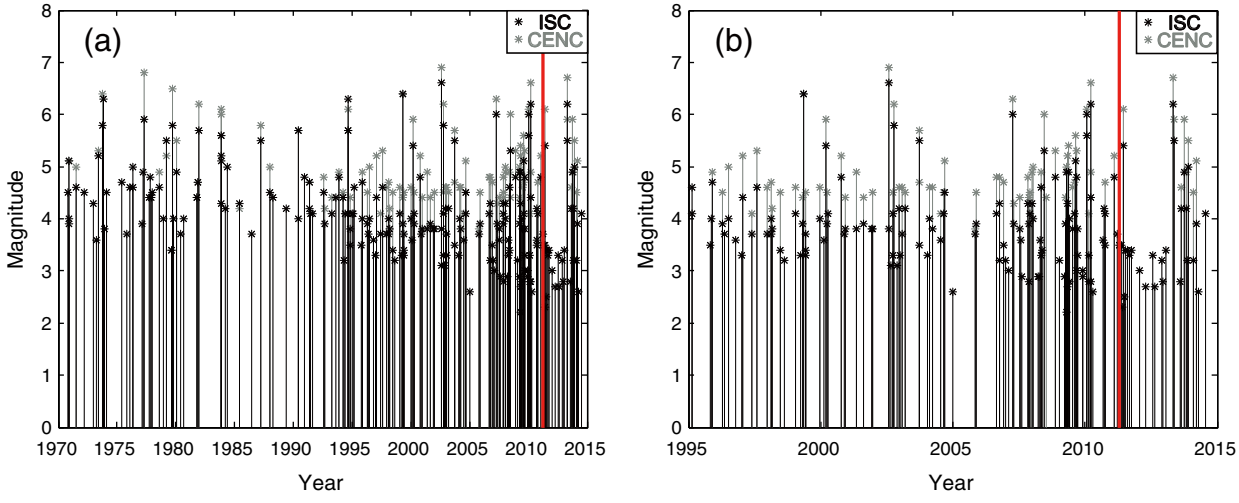

Fig. 5. (a) Deep-focus earthquakes (>350 km) in Northeast China during 1970 and 2014. Each black and gray asterisk represents an earthquake reported by ISC and CENC, respectively. The red line marks the 2011 Tohoku-Oki earthquake. (b) Same as (a) but for the period from 1995 to 2014.

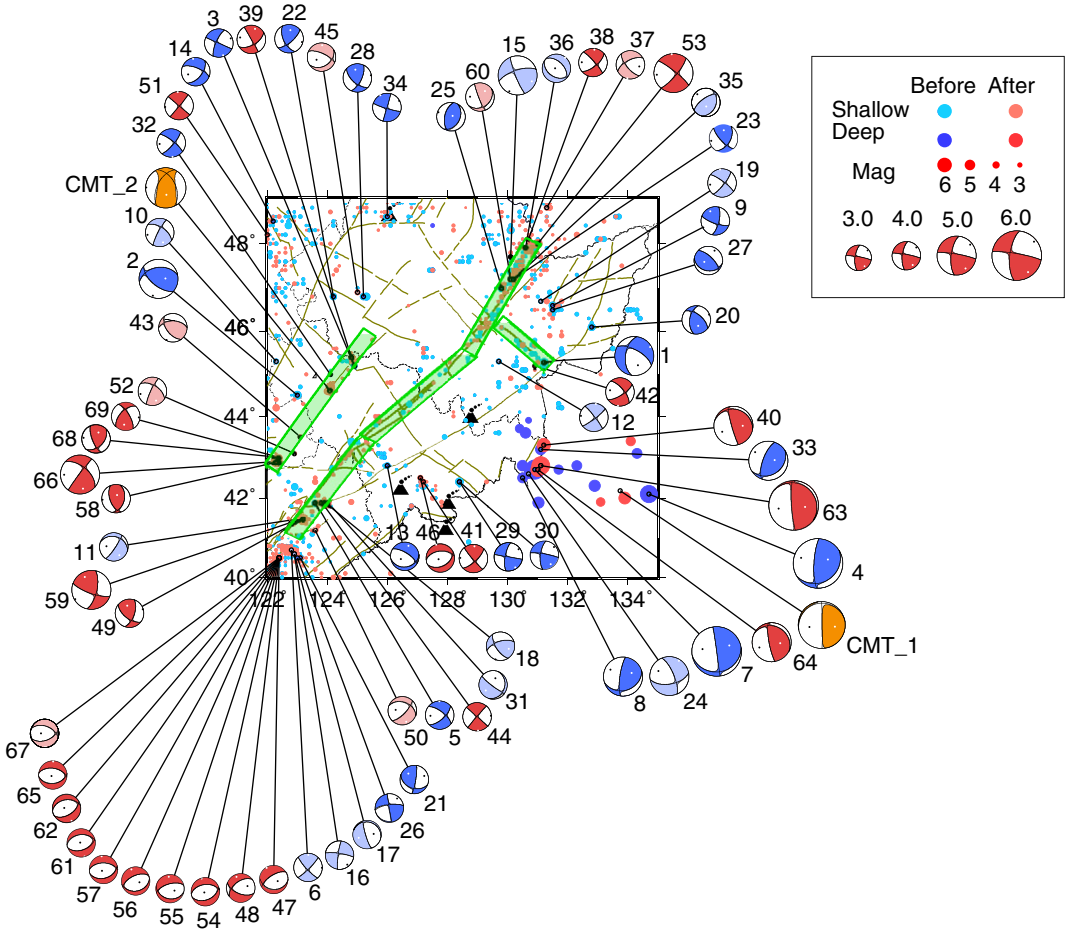

Fig. 6. The lower-hemisphere stereographic projections (beachballs) of 69 earthquakes ($2.9 \le M_W \le 6.8$) from December 2009 to May 2013 determined in this study. Two orange beachballs are events happened after May 2013 reported by GCMT solutions. Blue and red beachballs represent earthquakes before and after the 2011 Tohoku earthquake, respectively, with lighter colors indicating focal mechanisms of lower qualities. Seismicity distribution and green belts marking main fault zone are the same as in Fig. 4(a).

minor details of different co-seismic slip models do not matter much in our Coulomb stress calculation. Here we use the co-seismic slip model from Yue and Lay (2011) derived from high-rate GPS data. We vary the Coulomb frictional coefficient μ between 0.2–0.8, and show the case for 0.4 (Fig. 8) which best describes the seismicity change on the major faults (see Fig. S2 in supplementary material for details); the choice of $\mu = 0.4$ is

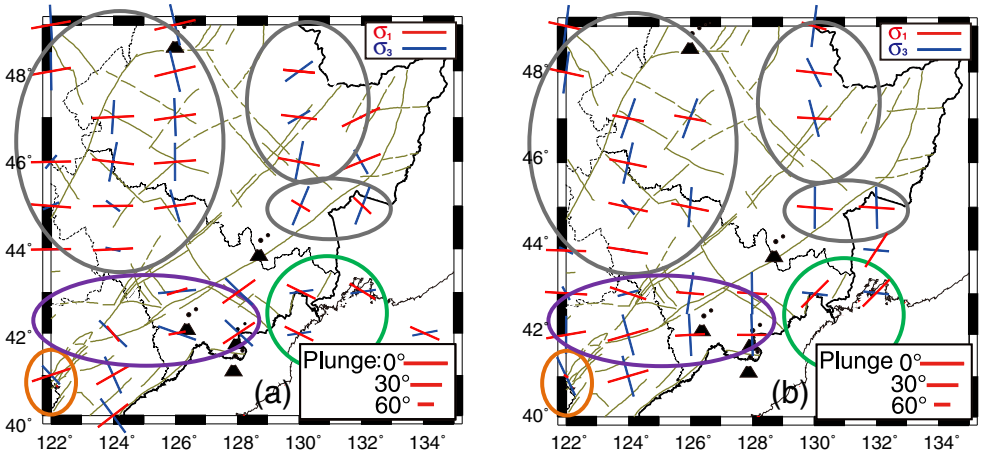

Fig. 7. (a) Result of the stress field inversion using the FMSs of the 36 events before the 2011 Tohoku earthquake. The horizontal grid has a uniform grid spacing of 2.0° and 1.0° in longitude and latitude, respectively. Horizontal projections of the principle stress axes σ_1 (maximum compression) and σ_3 (minimum compression) are plotted at each resolvable grid point with red and blue line segments, respectively. (b) Same as (a) but using the 33 earthquakes after the Tohoku-Oki earthquake. Colored ellipses indicate different patterns of stress state in the region: In gray ellipses, the direction of maximum compression rotated from roughly E–W to WNW–ESE; in purple ellipses, the direction of σ_1 became more-or-less horizontal and oriented roughly E–W; in orange ellipses, the direction of σ_1 became almost vertical; and in green ellipses, the direction of σ_1 indicated by the mantle-depth earthquakes changed from WNW–ESE to WSW–ENE.

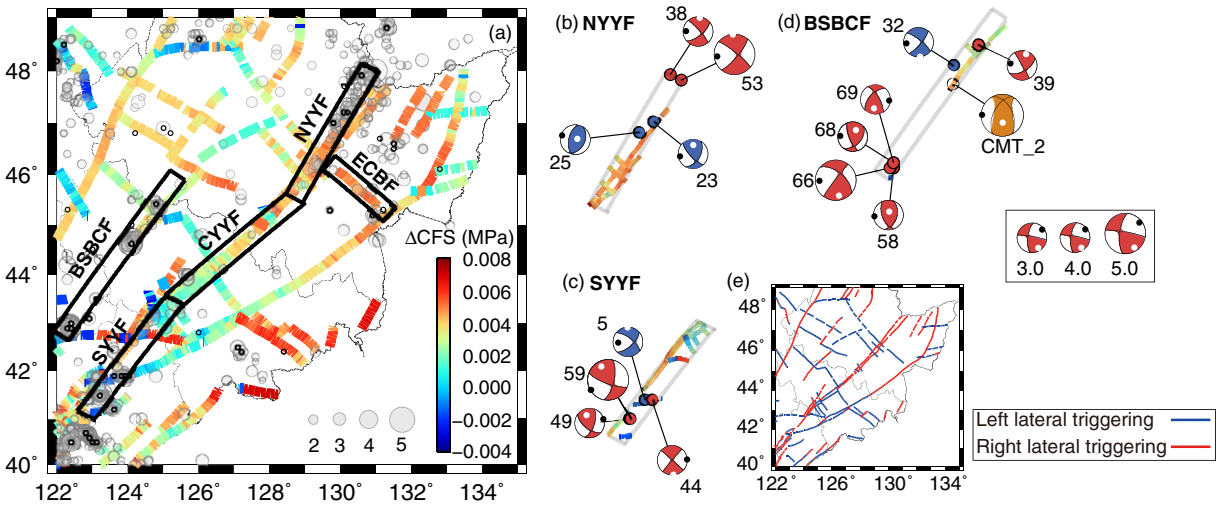

Fig. 8. Static Coulomb stress change calculation and FMSs. (a) Static Coulomb stress change on the major faults within the Northeast China due to the 2011 Tohoku-Oki earthquake, calculated at the depth of 10 km (We test at depths 5 km, 10 km and 15 km, but find the difference is minimal, shown as Fig. S3. And 10 km is also a reasonable assumption of crustal seismicity depths). The megathrust slip model is from Yue and Lay (2011). The regional stress is set to 10 MPa in the E–W direction and we choose a value of 0.4 for the frictional coefficient. Colors of the faults represent the coseismic static Coulomb stress change, taking the strike–slip faults' left-lateral or right-lateral properties into account. Gray circles depict the cataloged events occurring after the 2011 Tohoku-Oki earthquake. Black circles are for crustal-depth events for which we calculated focal mechanisms. (b)–(d) Details for the NYYF, SYYF and BCSBF fault zones, color-coded in the same way as in (a). We also plot the FMSs determined in this study with blue and red beachballs for earthquakes before and after the megathrust event, respectively, using lower-hemisphere stereographic projections. Black and white dots on beachballs indicate the P and T axes, respectively. The orange beachball is the GCMT solutions an event occurring after May 2013. The sizes of beachballs are proportional to the moment magnitude and their IDs are chronologically numbered (see Table S1). (e) Preferred triggering mode of each fault resulting from the megathrust stress change, with blue for left-lateral slip triggering and red for right-lateral.

also representative of friction coefficient values adopted in most other △CFS calculations (e.g., King et al., 1994). Here we also assume that the maximum compressional principle axis is roughly horizontal and along E–W direction according to our stress state inversions and previous studies (Ning and Zang, 1987; Xu, 2001), and that the maximum extensional principal axis in this region is also horizontal.

As shown in Fig. 8(a), the △CFS is no more than 0.01 MPa in the NEC region, which is roughly in accordance with a recent study on the influence of the 2011 Tohoku megathrust earthquake in eastern China (Cheng et al., 2014). In addition, the radial pattern and stress amplitude variation based on the Coulomb Failure Stress change calculation is consistent with the horizontal deformation of the 2011 Tohoku-Oki earthquake (see Fig. 2(b) of Tregoning et al., 2013). Despite the small △CFS values, they can still predict to the first degree the changes of seismicity rate. △CFS is larger on NYYF and SYYF than on CYYF, where we show in Fig. 4(b) that seismicity rate along the Yilan–Yitong Fault (YYF) has increased on its northern and southern segments (NYYF and SYYF) but decreased on the central part (CYYF). This difference in the seismicity rate change along the three YYF segments may be explained by their different fault strike orientations. Both NYYF and SYYF have strikes closer to N–S than CYYF, which would result in a larger reduction in normal stress and a smaller reduction in shear stress, hence moving closer to the Coulomb failure criteria. According to the seismicity distribution, a buried right-lateral fault (BCSBF) seems to extend parallel to SYYF in Fig. 8(a). Since it also has a nearly N–S strike, it would tend to induce a larger △CFS, and hence a seismicity increase after the megathrust event.

However, Coulomb stress changes on some faults do not match their seismicity rates after the Tohoku-Oki earthquake. One of the possible reasons is that we have used a spatially uniform frictional coefficient while in reality it may vary among individual faults. Given the same reduction of E–W compressional stress ($\Delta\sigma_n$), a larger frictional coefficient would lead to larger Coulomb stress changes (see supplementary material Fig. S2).

In the eastern part of Chenshu–Boli Fault (ECBF), the decrease in seismicity rate (Fig. 4b) is in contrast to the increase in Coulomb stress. It is possible that some stress in the area had been released during a M_L 4.5 earthquake that occurred on December 19, 2009, along ECBF. Hence the Coulomb stress increase due to the Tohoku-Oki earthquake was not big enough to accelerate further seismicity, despite the fact that it is the highest for the cases shown in Fig. 8(a). Moreover, seismicity became sparse along ECBF two months after the megathrust event (see Fig. S2 in supplementary material). Comparing with the other fault zones that have smaller △CFS and instant seismic response to the 2011 Tohoku-Oki earthquake, we consider the low seismicity in ECBF area is a result of local effects but not related to the Tohoku-Oki earthquake.

We illustrate in Fig. 8(b–d) the FMSs of earthquakes located around the NYYF, SYYF and BCSBF fault zones (black boxes in Fig. 8a) from December 2009 to May 2013 using the lower-hemisphere stereographic projections. The FMSs of earthquakes occurring along the faults NYYF, SYYF and BCSBF agree well with the strikes of the faults, suggesting that the △CFS on the strike–slip faults can be a good indicator for the influence on the stress state by the megathrust event, as shown in Fig. 8(b)–(d).

Moreover, the value of △CFS decreases with epicentral distance in general (Fig. 8a). The westward reduction is also consistent with the results that the northwest corner of our research area does not have as much variation in both seismicity and stress state as in the eastern part (Figs. 4 and 7). Besides, the stress perturbation effect is more notable on right-lateral faults (striking NE–SW) than on left-lateral ones (striking NW–SE) based on the seismicity change on the major faults (Fig. 4a). Our inferred faulting types (left-lateral or right-lateral), as shown in Fig. 8(e), are in accordance with the geological evidence from paleoseismicity studies (Xu and Deng, 1996).

3.4. FMSs at mantle-depth

To verify whether the FMSs of mantle-depth earthquakes determined in this study have a systematic change in the horizontal components of P axes after the 2011 Tohoku-Oki earthquake, we compare our result with 23 GCMT solutions for deep-focus earthquakes in the same region from January 1976 up to the 2011 Tohoku-Oki earthquake (see Table S3 in supplementary material for details). In general, the directions of the horizontal components of P axes before the 2011 Tohoku-

Oki earthquake are predominantly WNW–ESE, consistent with the subduction direction. Only three GCMT solutions have P axes with horizontal components in WSW–ENE direction (see Table 1 for details). After the megathrust event, P axes rotated anticlockwise to WSW–ENE, as shown in Figs. 4(d) and 9(a), although some margin of errors in the moment tensor solutions cannot be ruled out due to limited observations.

We further investigate the features of mantle-depth events in the cross-sectional view. Fig. 9(b) shows the projection of events in the dashed black box in Fig. 9(a) on to the vertical cross-section marked by the thick black line). Events reported by the ISC catalog between 1970 and 2011 (before the megathrust earthquake) delineate the subducting Pacific Plate below NEC (gray dots in Fig. 9b). Earthquakes in the cross-section mainly gather in two clusters, at the depths from 420 km to 460 km and from 520 km to 580 km.

Their FMSs fall into two groups based on the orientations of their P axes. Group 1 events have P axes parallel to the dip direction of the subducting Pacific Plate (events #1, 4, 6–7, 9 and 11–13, red or blue circles with black outlines in Fig. 9b), whereas the P axes of Group 2 events are more horizontal and along the trench (perpendicular to the cross-section in 8(b); events #2–3, 5, 8 and 10, blue circles with red outlines). The three events that occurred after the 2011 Tohoku-Oki earthquake (#11–13) and events above the deeper cluster (#1, 4 and 6) belong to Group 1, while majority of the events in Group 2 delineate the outer margin of the deeper cluster. The magnitudes of Group 1 earthquakes are generally larger than those of Group 2. T axes of most events are perpendicular to the dip direction of the subducting plate (in cross-sectional view), except for events #4, 9, which have horizontal T axes along the trench (that is, roughly parallel to the P axes of Group 2 events). Moreover, Fig. 9(b) provides more details on the seismic gap mentioned in Section 3.1. At the depth range of the deeper cluster, there are no events detected between the occurrence times of events #11 and #12, as the color bar in Fig. 9(b) shows. In the meantime, only smaller events occurred during these two years at shallower depth.

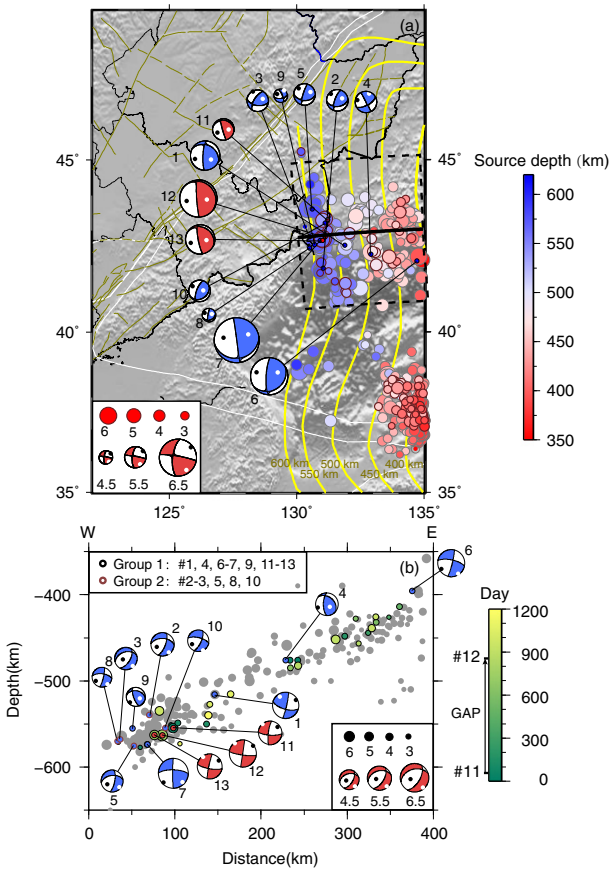

Fig. 9. Distribution and FMSs of mantle-depth earthquakes. (a) The FMSs of 11 earthquakes between May 2008 and May 2013 determined using gCAP in this study are plotted in blue (before Tohoku earthquake) and red (after Tohoku earthquake) beachballs. Gray and brown circles show respectively events reported by the ISC catalog happened before and after the 2011 Tohoku-Oki earthquake, with sizes proportional to magnitudes and fill-in colors representing focal depths. Thick black line and dashed box mark the location of cross-section in (b) and its projection area, respectively. Yellow curves in (a) depict the iso-depth contours of the Pacific subducting slab. (b) Cross-section showing vertical distribution of deep-focus events. Horizontal and vertical ordinate respectively show the distance from the west endpoint of the profile marked in (a) and the depth. FMSs are the same as in (a) but projected to the vertical profile. Gray dots are events reported by the ISC catalog occurred before the 2011 Tohoku-Oki earthquake. Dots with green to yellow fill-in colors show the origin time of events relative to the mega thrust event. The seismic gap of moderate earthquakes between May 2011 and April 2013 is marked on the color bar. Blue dots with black edges mark Group 1 earthquakes with the orientations of P axes perpendicular to the iso-depth contours, whereas those with pink edges mark Group 2 events with P axes parallel to the iso-depth contours.

4. Discussion

The 2011 Tohoku-Oki earthquake increased the global seismicity rates for at least several days (Gonzalez-Huizar et al., 2012). In Northeast Asia, the influence of the megathrust event on the regional focal mechanism solutions (FMSs) may last for several years to decades due to the perturbation to the stress field (Wang et al., 2012). Our analyses here focus on elastic response to the megathrust coseismic slip for two reasons. First, the coseismic slip in the NEC area induced by the 2011 Tohoku-Oki earthquake is equivalent to 12.7 years of cumulative background strain, based on the estimation of GPS observation (Chen et al., 2012), which may result in accelerated seismicity, as we have observed in this study. Second, the earthquakes we study here are either at crustal-depth (<35 km) or within the subducting plate at the mantle depths, where elastic properties should still dominate at the short 4-year postseismic time scale. Therefore, our discussion will focus on the effects of the coseismic slip of the 2011 Tohoku-Oki earthquake, taking the NEC region as an example to show how a distant M_W 9 earthquake impacts on the seismicity, earthquake focal mechanisms and stress state.

The overall seismicity rate in the NEC did not change significantly after the 2011 Tohoku-Oki earthquake, which is reasonable since the distance to the source area is more than 1200 km and the change of static Coulomb stress is less than 0.01 MPa. Nevertheless, the change in the number of earthquakes on the major faults, in particular on the NEN–SWS striking faults, is not negligible. As shown in Section 3.1, the number of events along the NYYF, SYYF and BCSBF faults increased while it decreased along faults CYYF and ECBF.

Meanwhile, the characteristics of the FMSs before the 2011 Tohoku-Oki earthquake vary from one place to another. Such observations, along with the relatively low seismicity and the small to moderate magnitudes of the events, indicate a low-level background stress within the NEC region. After the megathrust event, the shallow earthquakes can mainly be divided into two groups, strike–slip events with compressional stress oriented E–W and normal-fault events with extensional stress pointing N–S, as shown in Fig. 6.

The first group, strike–slip events with E–W compressional axes, is the dominant type in the NEC region after the megathrust event. It is probable that the nearly E–W (direction of the P axis of the Tohoku-

Table 1
Information on three deep-focus events before the 2011 Tohoku-Oki earthquake in GCMT catalog showing WSW–ENE-oriented P axes, with right-lateral strike–slip FMS to the events occurring after the 2011 Tohoku-Oki earthquake.

Date	Longitude (°)	Latitude (°)	Depth (km)	Magnitude (M_w)	Azimuth of P axes (°)
1983-10-08	130.39	44.18	573	6.1	261.00
2008-05-19	131.96	42.51	530	5.9	240.83
2009-03-13	133.91	43.37	445	4.8	259.96

Oki earthquake) extension caused by the megathrust event to our study area has the effect of changing the normal and shear stresses of existing faults in North China and triggers strike–slip events. As Fig. 10 illustrates, the E–W extension due to the Tohoku-Oki earthquake unloads the faults, leading to a decrease in both normal and shear stresses (positive for compression). When the decrease in normal stress is greater than that of the decrease in shear stress (strike φ close enough to N–S direction), Coulomb stress increases. If we consider the stress change in the context of a Mohr circle diagram, the Coulomb–Mohr circle moves closer to the Coulomb failure envelope in this scenario. The static △CFS calculation provides a quantitatively consistent result. The positive values of the calculated static Coulomb stress changes on faults within gray and purple ellipses in Fig. 7(b) can well explain the strike–slip events there with E–W compression after the 2011 Tohoku-Oki earthquake, which also agrees with our stress inversion results.

The second group of earthquakes also results from the additional E–W tensile stress. Before the megathrust event, the maximum compressional principle stress within the orange ellipses in Fig. 7 is roughly E–W, which agrees with the background stress. The 2011 Tohoku-Oki earthquake triggered a roughly E–W tensile stress on the original low-level E–W compressional background stress field, which decreases the previous maximum compressional principle stress. The maximum principle stress thus became more vertical, a favorable condition for N–S tensile normal-faulting earthquakes.

In summary, an M_W 9 megathrust earthquake may not have a noticeable influence on the overall seismicity rate on regional scale of distance more than 1200 km away. However, for tectonic faults where stress state is near critical for earthquake faulting, even a small perturbation in the stress field can result in accelerated seismicity, depending on the location, strike, dip, rake, and frictional properties of the faults. In the NEC, faults with strikes parallel to the Japan Trench, nearly vertical dipping, higher friction coefficient and critically stressed are all favorable conditions for the triggering of seismic slip. In addition, we found that a △CFS of less than 0.01 MPa can influence the characteristics of the FMSs at crustal depths. Differences in focal mechanisms of crustal earthquakes after the Tohoku earthquake are probably due to the variation in the local stress state. In this study, the roughly E–W compressional stress is smaller in areas with primarily N–S extensional normal-faulting events than in other areas of the NEC region.

On the other hand, compressional stress in the Pacific Plate due to tens of meters of interplate movement near the Japan Trench would be transferred down to mantle depths along the plate. Since the 2011 Tohoku-Oki earthquake is a low-angle megathrust event, the direction of stress transfer is mainly down-dip. In cross-sectional view, the stress in the dip direction gets strengthened in the subducting plate. Before the megathrust earthquake, we observe two groups of mantle-depth FMSs as shown in Fig. 9(b): 1) P axes parallel to the dip direction; and 2) P axes parallel to the slab strike. The stress perturbation due to the megathrust event is thus favorable for promoting Group 1 events by increasing the maximum principle stress along dip, meanwhile inhibits Group 2 events. Distribution of deep-focus events after the megathrust earthquake does agree with the effect of the stress perturbation. In fact, all three events after the 2011 Tohoku-Oki earthquake belong to Group 1. As Fig. 9(b) shows, Group 2 events tend to occur at the outer margin of the deeper cluster while Group 1 events are aligned inside the shallower and deeper clusters. The lack of moderate (~M_W 4–5) events in the deeper cluster between May 2011 and April 2013 may be partly due to the suppression of Group 2 events, which are mostly of medium sizes. In addition, we consider that the M_W 5.4 event on May 10, 2011 (event #11) is highly related to the stress variation of the 2011 Tohoku-Oki earthquake (Li et al., 2013). This earthquake probably released a significant amount of stress at depth. All the aforementioned factors may have led to the quiescence of M_W 4–5 earthquakes until a M_W 6.2 earthquake occurred on April 5, 2013 (event #12), which may have triggerred other earthquakes due to stress adjustment. The seismicity at depth then subsequently resumed, as seen in Fig. 5(b).

Some statistical studies have proposed that megathrust events in the Japan Trench have a delayed positive correlation on the time scale of years with increased seismicity at mantle depths in the NEC region (Wu et al., 1979; Li and Wang, 1996; Gao, 2011), probably also implying the role of stress perturbation along the subducting Pacific Plate. Our study is the first to focus on the short-time scale (right after the 2011 Tohoku-Oki earthquake) influence of a megathrust event on both the seismicity and FMSs at mantle depths 1200 km away. Further work is required to confirm our conjecture and to reveal the details of how a shallow megathrust event may lead to a seismicity gap and earthquakes at the mantle depth with preferred orientation of P axes. Related studies about dynamic rupture processes of mantle-depth earthquakes in the NEC region, such as those for the May 24, 2013, M_W 8.3 Sea of Okhotsk earthquake (Zhan et al., 2014; Ye et al., 2013; Meng et al., 2014), will shed light on the mechanism of NEC deep-focus earthquakes.

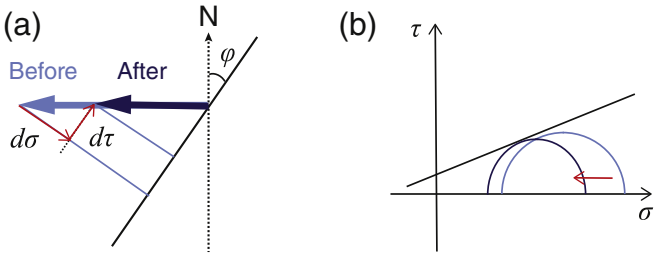

Fig. 10. Sketch for the stress change on a fault of strike φ. (a) Light and dark blue arrows represent the maximum compressional principle stresses before and after the 2011 Tohoku-Oki earthquake, respectively. Red arrows indicate the change of normal and shear stresses on the fault. (b) Mohr circle diagram of the stress field. As the red arrow illustrates, the regional stress change due to the 2011 Tohoku-Oki earthquake may increase the chance of fault rupture in Northeast China by moving the Mohr circle closer to the Coulomb failure criterion line.

5. Conclusion

Using the waveform records between 2009 and 2013 from the CEA, NECESSARRAY, and NECSAIDS arrays, we determine the focal mechanism solutions of 69 earthquakes that occurred in the NEC at both crustal and mantle depths. Comparisons of the focal mechanisms and seismicity rate in the NEC before and after the 2011 Tohoku-Oki earthquake reveal that, except along the major active faults, seismicity did not change significantly at crustal depths, which is consistent with the result of the static Coulomb stress change generally less than 0.01 MPa. After the megathrust earthquake, the number of events increased along northern Yilan–Yitong Fault (NYYF), southern YYF (SYYF), and buried Central Songliao Basin Fault (BCSBF) while decreased along the central part of the YYF (CYYF). The static Coulomb stress change is larger on NYYF and SYYF than on CYYF. The FMSs of shallow events can mainly be divided into two groups after the megathrust event: strike–slip events with E–W compressional axes and normal-faulting events with N–S extensional axes. Based on these results, we conclude that for the strike–slip events, a roughly E–W extensional force (in the direction of the Tohoku-Oki earthquake P axis) caused by the megathrust event has changed the normal and shear stresses on major active faults in the NEC and accelerated seismicity on them. On the other hand, the megathrust earthquake superimposed a roughly E–W extensional stress on the original low-level E–W compressional background stress, which changed the maximum compressional principle stress to a vertical direction and hence facilitated the N–S extension of the normal-faulting events.

After the megathrust event, moderate-sized mantle-depth earthquakes (~M_W 4–5) were absent in the NEC between May 2011 and April 2013, possibly due to the local stress release by an Mw 5.4 event. Tens of meters of interplate coseismic movement at shallow depth in

the trench area may have led to a noticeable down-dip transfer of compressional stress in the Pacific Plate. Thus, the stress perturbation at mantle depth may have facilitated the events with P axes parallel to the dip of the subducting Pacific Plate in cross-sectional view and oriented WNW–ESE in map view.

Acknowledgments

Data used in this study are obtained from the ISC, NECESSArray group, NECSAIDS group, GCMT group, CENC, and the Data Management Centre of China National Seismic Network at Institute of Geophysics, China Earthquake Administration (SEISDMC, doi:10.7914/SN/CB). We thank Rebecca M. Harrington, Jeff J. McGuire, Douglas A. Wiens and Alexander Carey for providing thoughtful comments and suggestions. This work was supported by the National Science Foundation of China under grant 41130316 (J.-Y. Ning and Q.-F. Chen). Figures are prepared using GMT (Wessel and Smith, 1998) and Matlab.

Appendix A. Supplementary data

Supplementary data to this article can be found online at http://dx.doi.org/10.1016/j.tecto.2015.10.009.

References

Ammon, C., Lay, T., Kanamori, H., Cleveland, M., 2011. A rupture model of the 2011 off the Pacific coast of Tohoku Earthquake. Earth Planets Space 63 (7), 693–696.
Aki, K., Richards, P., 2002. Quantitative seismology. Vol. 1.
Chen, W., Gan, W., Xiao, G., Liang, S., Sheng, C., 2012. The impact of 2011 Tohoku-Oki earthquake in Japan on crustal deformation of northeastern region in China. Dizhen Dizhi (Seismology and Geology, in Chinese) 34(3), pp. 425–439.
Cheng, J., Liu, M., Gan, W., Xu, X., Huang, F., Liu, J., 2014. Seismic impact of the M_W 9.0 Tohoku earthquake in Eastern China. Bull. Seismol. Soc. Am. 104 (3), 1258–1267.
Deng, Q., Ran, Y., Yang, X., Min, W., Chu, Q., 2007. Map of Active Tectonics in China. Seismol, Press, Beijing.
Dreger, D., Helmberger, D., 1993. Determination of source parameters at regional distances with single station or sparse network data. J. Geophys. Res. 98, 8107–8125.
Ekstrom, G., Nettles, M., Dziewonski, A., 2012. The global CMT project 2004–2010: centroid-moment tensor for 13,017 earthquakes. Phys. Earth Planet. Inter. 200–201, 1–9.
Fujii, Y., Satake, K., Sakai, S., Masanao, S., Kanazawa, T., 2011. Tsunami source of the 2011 off the Pacific coast of Tohoku, Japan earthquake. Earth Planets Space 63 (7), 815–820.
Gao, L., 2011. Dynamic background and space-time characteristics analysis of earthquake activities in Northeast China. Earthquake 31 (1), 41–51 (in Chinese with English abstract).
Gonzalez-Huizar, H., Velasco, A., Peng, Z., Castro, R., 2012. Remote triggered seismicity caused by the 2011, M9.0 Tohoku-Oki, Japan earthquake. Geophys. Res. Lett. 39 (10).
Hardebeck, J., Michael, A., 2006. Damped regional-scale stress inversions: methodology and examples for southern California and the Coalinga aftershock sequence. J. Geophys. Res. 111, B11310. http://dx.doi.org/10.1029/2005JB004144.
Hayes, G., 2011. Rapid source characterization of the 2011 M_W 9.0 off the Pacific coast of Tohoku Earthquake. Earth Planets Space 63 (7), 529–534.
Herrmann, R.B., Benz, H., Ammon, C.J., 2011. Monitoring the earthquake source process in North America. Bulletin of the Seismological Society of America 101 (6), 2609–2625.
Hiratsuka, S., Sato, T., 2011. Alteration of stress field brought about by the occurrence of the 2011 off the Pacific coast of Tohoku earthquake (M_W 9.0). Earth Planets Space 63 (7), 681–685.
Huang, J., Zhao, D., 2006. High-resolution mantle tomography of China and surrounding regions. J. Geophys. Res. 111, B09305. http://dx.doi.org/10.1029/2005JB004066.
Hwang, J., Yun, H., Huang, H., Jung, T., Lee, D., We, K., 2012. The 2011 Tohoku-Oki earthquake's influence on the Asian plates and Korean geodetic network. Chin. J. Geophys. 55 (6), 1884–1893.
Ito, Y., Tsuji, T., Osada, Y., Kido, M., Inazu, D., Hayashi, Y., Tsushima, H., Hino, R., Fujimoto, H., 2011. Frontal wedge deformation near the source region of the 2011 Tohoku-Oki earthquake. Geophys. Res. Lett. 38, L00G05. http://dx.doi.org/10.1029/2011GL048355.
Kennett, B., Engdahl, E., Buland, R., 1995. Constraints on seismic velocities in the Earth from traveltimes. Geophys. J. Int. 122 (1), 108–124.
King, G., Stein, R., Lin, J., 1994. Static stress changes and the triggering of earthquakes. Bull. Seismol. Soc. Am. 84 (3), 935–953.
Li, X., Wang, W., 1996. Correlation analysis of earthquakes in the North China and Japan sea trench. Earthquake 3, 001.
Li, S., Chen, Q., Zhao, L., Zhu, L., Gao, J., Li, M., Liu, G., Wang, B., 2013. Anomalous focal mechanism of the May 2011 Mw 5.7 deep earthquake in Northeastern China: regional waveform inversion and possible mechanism. Chin. J. Geophys. 56 (9), 2959–2970. http://dx.doi.org/10.6038/cjg20130910 (in Chinese).
Lin, J., Stein, R., 2004. Stress triggering in thrust and subduction earthquakes, and stress interaction between the southern San Andreas and nearby thrust and strike–slip faults. J. Geophys. Res. 109, B02303. http://dx.doi.org/10.1029/2003JB002607.
Lund, B., Townend, J., 2007. Calculating horizontal stress orientations with full or partial knowledge of the tectonic stress tensor. Geophys. J. Int. 170 (3), 1328–1335. http://dx.doi.org/10.1111/j.1365-246X.2007.03468.x.
Martínez-Garzón, P., Kwiatek, G., Ickrath, M., Bohnhoff, M., 2014. MSATSI: a MATLAB© package for stress inversion combining solid classic methodology, a new simplified user-handling and a visualization tool. Seismol. Res. Lett. 85 (4), 896–904. http://dx.doi.org/10.1785/0220130189.
Meng, L., Ampuero, J., Bürgmann, R., 2014. The 2013 Okhotsk deep-focus earthquake: Rupture beyond the metastable olivine wedge and thermally controlled rise time near the edge of a slab. Geophys. Res. Lett. 41, 3779–3785. http://dx.doi.org/10.1002/2014GL059968.
Michael, A., 1984. Determination of stress from slip data: faults and folds. J. Geophys. Res. 89, 11,517–11,526.
Ning, J., Zang, S., 1987. The distribution of earthquakes and stress state in the Japan Sea and the northeast China. Seismol. Geol. 2, 009.
Patton, H., Zandt, G., 1991. Seismic moment tensors of western U.S. earthquakes and implications for the tectonic stress field. J. Geophys. Res. 96, 18,245–18,259.
Romanowicz, B., Dreger, D., Pasyanos, M., Uhrhammer, R., 1993. Monitoring of strain release in central and northern California using broadband data. Geophys. Res. Lett. 20, 1643–1646.
Shao, G., Li, X., Ji, C., Maeda, T., 2011. Focal mechanism and slip history of the 2011 M_W 9.1 off the Pacific coast of Tohoku Earthquake, constrained with teleseismic body and surface waves. Earth Planets Space 63 (7), 559–564.
Shestakov, N., Takahashi, H., Ohzono, M., Prytkov, A., Bykov, V., Gerasimenko, M., Serov, M.A., 2012. Analysis of the far-field crustal displacements caused by the 2011 Great Tohoku earthquake inferred from continuous GPS observations. Tectonophysics 524, 76–86.
Simons, M., Minson, S., Sladen, A., Ortega, F., Jiang, J., Owen, S., Meng, L., Ampuero, J., Wei, S., Chu, R., Helmberger, D., Kanamori, H., Hetland, E., Moore, A., Webb, F., 2011. The 2011 magnitude 9.0 Tohoku-Oki earthquake: mosaicking the megathrust from seconds to centuries. Science 332, 1421–1425. http://dx.doi.org/10.1126/science.1206731.
Sun, Y., 2005. P- and S-wave tomography of the crust and uppermost mantle in China and surrounding areas Ph.D. thesis Mass. Inst. of Technol, Cambridge.
Toda, S., Stein, R., Richards-Dinger, K., Bozkurt, S., 2005. Forecasting the evolution of seismicity in southern California: animations built on earthquake stress transfer. J. Geophys. Res. 110, B05S16. http://dx.doi.org/10.1029/2004JB003415.
Toda, S., Stein, R., Sevilgen, V., Lin, J., 2011a. Coulomb 3.3 Graphic-rich deformation and stress-change software for earthquake, tectonic, and volcano research and teaching-user guide. U.S. Geological Survey Open-File Report 2011–1060 (63 pp., available at http://pubs.usgs.gov/of/2011/1060/).
Toda, S., Lin, J., Stein, R., 2011b. Using the 2011 M = 9.0 Tohoku earthquake to test the Coulomb stress triggering hypothesis and to calculate faults brought closer to failure. Earth Planets Space 63 (7), 725–730.
Toda, S., Stein, R., Lin, J., 2011c. Widespread seismicity excitation throughout central Japan following the 2011 M = 9.0 Tohoku earthquake and its interpretation by Coulomb stress transfer. Geophys. Res. Lett. 38, L00G03. http://dx.doi.org/10.1029/2011GL047834.
Tregoning, P., Burgette, R., McClusky, S., Lejeune, S., Watson, C., McQueen, H., 2013. A decade of horizontal deformation from great earthquakes. J. Geophys. Res. Solid Earth 118, 2371–2381. http://dx.doi.org/10.1002/jgrb.50154.
Wang, M., Li, Q., Wang, F., Zhang, R., Wang, Y., Shi, H., Zhang, P., Shen, Z., 2011. Far-field coseismic displacements associated with the 2011 Tohoku-oki earthquake in Japan observed by Global Positioning System. Chin. Sci. Bull. 56 (20), 1593–1596.
Wang, K., Hu, Y., He, J., 2012. Deformation cycles of subduction earthquakes in a viscoelastic Earth. Nature 484 (7394), 327–332.
Wessel, P., Smith, W., 1998. New, improved version of the Generic Mapping Tools released. Eos. Trans. AGU 79, 579.
Wu, J., Yu, S., He, S., 1979. The correlation of earthquake occurrence between Northeastern China and Japan. Chin. J. Geophys. 22 (04), 415–438.
Xu, Z., 2001. A present-day tectonic stress map for eastern Asia region. Acta Seismol. Sin. 14 (5), 524–533.
Xu, X., Deng, Q., 1996. Nonlinear characteristics of paleoseismicity in China. J. Geophys. Res. Solid Earth (1978–2012) 101 (B3), 6209–6231.
Ye, L., Lay, T., Kanamori, H., Koper, K., 2013. Energy release of the 2013 M_W 8.3 Sea of Okhotsk earthquake and deep slab stress heterogeneity. Science 341 (6152), 1380–1384.
Yue, H., Lay, T., 2011. Inversion of high-rate (1 sps) GPS data for rupture process of the 11 March 2011 Tohoku earthquake (M_W 9.1). Geophys. Res. Lett. 38, L00G09. http://dx.doi.org/10.1029/2011GL048700.
Zhan, Z., Kanamori, H., Tsai, V., Helmberger, D., Wei, S., 2014. Rupture complexity of the 1994 Bolivia and 2013 Sea of Okhotsk deep earthquakes. Earth Planet. Sci. Lett. 385, 89–96.
Zhao, L., Helmberger, D., 1994. Source estimation from broadband regional seismograms. Bull. Seismol. Soc. Am. 84, 91–104.
Zheng, X., Yao, Z., Liang, J., Zheng, J., 2010. The role played and opportunities provided by IGP DMC of China National Seismic Network in Wenchuan earthquake disaster relief and researches. Bull. Seismol. Soc. Am. 100 (5B), 2866–2872. http://dx.doi.org/10.1785/0120090257.
Zhu, L., Ben-Zion, Y., 2013. Parametrization of general seismic potency and moment tensors for source inversion of seismic waveform data. Geophys. J. Int. 194 (2), 839–843.
Zhu, L., Helmberger, D., 1996. Advancement in source estimation techniques using broadband regional seismograms. Bull. Seismol. Soc. Am. 86, 1634–1641.
Zhu, L., Rivera, L., 2002. A note on the dynamic and static displacements from a point source in multilayered media. Geophys J. Int. 148 (3), 619–627.